



## ISTITUTO NAZIONALE DI RICERCA METROLOGICA Repository Istituzionale

A Molecule-Based Single-Photon Source Applied in Quantum Radiometry

*Original*

A Molecule-Based Single-Photon Source Applied in Quantum Radiometry / Lombardi, Pietro; Trapuzzano, Marco; Colautti, Maja; Margheri, Giancarlo; Degiovanni, Ivo Pietro; López, Marco; Kück, Stefan; Toninelli, Costanza. - In: ADVANCED QUANTUM TECHNOLOGIES. - ISSN 2511-9044. - 3:2(2019), p. 1900083. [10.1002/qute.201900083]

*Availability:*

This version is available at: 11696/61628 since: 2020-02-28T11:17:18Z

*Publisher:*

*Published*

DOI:10.1002/qute.201900083

*Terms of use:*

This article is made available under terms and conditions as specified in the corresponding bibliographic description in the repository

*Publisher copyright*

(Article begins on next page)

# A Molecule-Based Single-Photon Source Applied in Quantum Radiometry

Pietro Lombardi, Marco Trapuzzano, Maja Colautti, Giancarlo Margheri, Ivo Pietro Degiovanni, Marco López, Stefan Kück, and Costanza Toninelli\*

Single-photon sources (SPSs) based on quantum emitters hold promise in quantum radiometry as metrology standard for photon fluxes at the low light level. Ideally this requires control over the photon flux in a wide dynamic range, sub-Poissonian photon statistics, and narrow-band emission spectrum. In this work, a monochromatic SPS based on an organic dye molecule is presented, whose photon flux is traceably measured to be adjustable between 144 000 and 1320 000 photons per second at a wavelength of  $(785.6 \pm 0.1)$  nm, corresponding to an optical radiant flux between 36.5 and 334 fW. The high purity of the single-photon stream is verified, with a second-order autocorrelation function at zero time delay below 0.1 throughout the whole range. Such molecule-based SPS is hence used for the calibration of a single-photon avalanche detector against a low-noise analog photodiode traceable to the primary standard for optical radiant flux (i.e., the cryogenic radiometer). Due to the narrow bandwidth of the source, corrections to the detector efficiency arising from the spectral power distribution are negligible. With this major advantage, the developed device may finally realize a low-photon-flux standard source for quantum radiometry.

## 1. Introduction

Sources of single photons are required for fundamental quantum optics experiments and are also key components in photonic quantum technologies.<sup>[1]</sup> Applications can be found in quantum cryptography,<sup>[2]</sup> quantum imaging,<sup>[3]</sup> simulation,<sup>[4]</sup> and quantum-enhanced optical measurements.<sup>[5]</sup> Notably, they turn out to be ideal sources for radiometry, especially in quantum radiometry, where low photon fluxes (in the fW range) have to be measured with low uncertainty. Indeed, current standards do not provide constant adjustable fluxes for calibrating single photon detectors and consequently all optical elements.<sup>[6]</sup> Even in the intermediate step of bridging the radiant power from single photon streams to the regime accessible with standard silicon photodiodes (calibrated against the primary standards), the problem of fluctuations in the average photon number per unit time

arises in the case of attenuated lasers<sup>[7,8]</sup> and a sub-Poissonian photon stream would be desirable.

In principle, single-photon sources (SPSs) offer the possibility to realize a new primary standard for light sources<sup>[9]</sup> in the low-flux range, complementing the blackbody radiator and the synchrotron radiation source. It is conceptually simple to relate the photon flux  $n$  with the energy flux, that is, the optical radiant flux (optical power)  $\phi$  through the simple expression  $\phi = n h \nu = n h c / \lambda$ , with  $h$  the Planck constant,  $c$  the speed of light,  $\nu$  the frequency, and  $\lambda$  the wavelength of the emitted radiation. In case of pulsed excitation and ideal photon source,  $n$  is exactly the pump repetition rate  $f$ , whereas for continuous wave (CW) pumping, the maximum average photon flux is essentially determined by the inverse of the excited state lifetime ( $1/\tau$ ). In both cases a sub-Poissonian photon stream is obtained whose variance can be related to the time-dependent Mandel's parameter as discussed in ref. [10]. Although in practice SPSs are never ideal due to the non-unitary collection and quantum efficiency, they may provide a reproducible photon flux once metrologically characterized. In fact, from the quantum theory of photodetection (see, e.g., ref. [11]), considering the photon count statistics measured in a time interval of  $\Delta t$ , the relationship between the variance in the measured photon flux  $(\Delta N)^2$  and the corresponding variance in the emitted photon flux  $(\Delta n)^2$  in the same time interval is given by  $(\Delta N)^2 = \eta^2 (\Delta n)^2 + \eta(1 - \eta) \langle n \rangle / \Delta t$ , where  $\eta$  is

Dr. P. Lombardi, Dr. C. Toninelli  
Istituto Nazionale di Ottica (CNR-INO)  
via N. Carrara 1, Sesto Fiorentino 50019, Florence, Italy  
E-mail: toninelli@lens.unifi.it


M. Trapuzzano  
Università degli Studi di Firenze  
via G. Sansone 1, Sesto Fiorentino 50019, Florence, Italy

M. Colautti  
LENS, Università degli Studi di Firenze  
via N. Carrara 1, Sesto Fiorentino 50019, Florence, Italy

Dr. G. Margheri  
Istituto dei Sistemi Complessi (CNR-ISC)  
via Madonna del Piano 10, Sesto Fiorentino 50019, Florence, Italy

Dr. M. López, Dr. S. Kück  
Physikalisch-Technische Bundesanstalt (PTB)  
Bundesallee 100, 38116 Braunschweig, Germany

Dr. I. P. Degiovanni  
Istituto Nazionale di Ricerca Metrologica (INRiM)  
Strada delle Caccie 91, 10135 Torino, Italy

 The ORCID identification number(s) for the author(s) of this article can be found under <https://doi.org/10.1002/qute.201900083>

© 2019 The Authors. Published by WILEY-VCH Verlag GmbH & Co. KGaA, Weinheim. This is an open access article under the terms of the Creative Commons Attribution License, which permits use, distribution and reproduction in any medium, provided the original work is properly cited.

DOI: 10.1002/qute.201900083

the overall emission, collection, and detection efficiency. In other words, the advantage of using photon Fock states with respect to weak coherent pulses, consists in a factor  $(1 - \eta)$  lower variance in the measured photon flux, since  $\frac{(\Delta N)_{\text{coherent}}^2}{(\Delta N)_{\text{Fock}}^2} = \frac{\eta(n)/\Delta t}{\eta(1-\eta)(n)/\Delta t} = \frac{1}{1-\eta}$

Few preliminary experiments in this direction have been performed with color centers in diamond. However, the source presented in ref. [12], for example, is based on an NV-center-doped nano-diamond at room temperature, and is hence not particularly suitable for application in single-photon detector calibration, because of the broad emission spectrum, ( $\Delta\lambda_{\text{FWHM}} \approx 100$  nm). A much narrower bandwidth source ( $\Delta\lambda_{\text{FWHM}} \approx 2$  nm) is reported in ref. [13], based on a silicon-vacancy center. In this case though, a direct calibration could not be carried out because of the low photon rate (60 kphoton/s), associated to an overall efficiency of  $\eta \approx 0.1\%$ . In this respect, sources based on semiconductor quantum dots<sup>[14]</sup> or molecules<sup>[15]</sup> in cryogenic environment look currently more suitable for applications. In particular, polycyclic aromatic hydrocarbon molecules show an unmatched combination of suitable properties in very simple experimental configurations: quantum yield close to unity, pronounced branching ratio in favor of the narrow-band zero phonon line (00-ZPL) at cryogenic temperature, and photostable emission.<sup>[16]</sup>

In this paper, we report on the optimized and metrologically characterized photon flux from a SPS based on a dibenzoterrylene (DBT) molecule in an anthracene (Ac) nanocrystal, exhibiting strong anti-bunching in the photon statistics, as well as narrow-band, bright, and photostable emission. Delivering more than 1 Mphoton/s at the detector under CW pumping, the source is effectively exploited for the calibration of a single-photon detector directly against a classical silicon photodiode. This is in turn traced to the primary standard for optical radiant flux, that is, the cryogenic radiometer. Based on the characterization and the radiometric experiments presented here, the developed molecule-based SPS might realize an absolute standard of low optical radiant fluxes.

The molecule-based SPS used for the experiments is described in Section 2. Section 3 deals with the metrological characterization of the source, while in Section 4 the SPS-based calibration of a silicon single-photon avalanche detector (SPAD) is discussed. In Section 5 we draw conclusions and outlooks, and in Section 6 the experimental steps are described in more detail.

Throughout the paper, with the expression “counts per second” (count/s) we refer to the count rate of a SPADs, while “photons per second” (photon/s) refers to the photon flux, evaluated as the count rate read by the detector divided by its quantum efficiency.

## 2. The Single-Photon Source

DBT molecules in Ac emit narrow-band photons when cooled down to cryogenic temperatures, exhibiting high quantum efficiency, photostability, and quantum coherence,<sup>[17,18]</sup> even embedded in small nanocrystals.<sup>[19]</sup> However, since a high photon flux is relevant for applications in quantum radiometry, collection efficiency of single molecule fluorescence requires optimization. This is particularly true for low numerical aperture (NA) optics, such as in the case of the long-working-distance microscope objective (NA = 0.67), which is used in the setup for cryogenic operation. In order to maximize the detected photon flux from

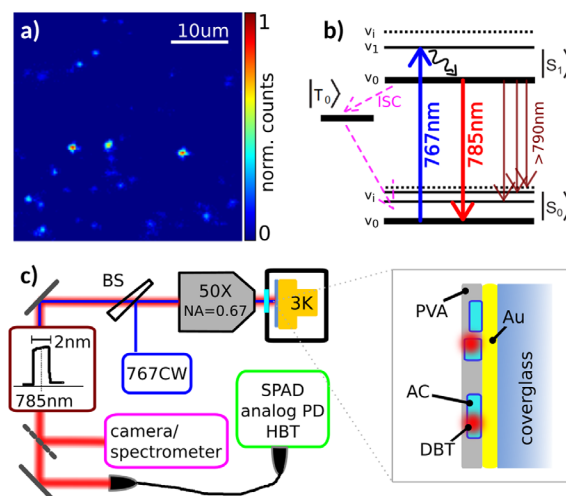


**Figure 1.** a) Wide-field (WF) fluorescence image: zoom ( $40 \times 40 \mu\text{m}^2$ ) on a region of the sample showing bright nanocrystals. b) Blue-detuned (767 nm) pumping scheme used to collect photons emitted into the 00-ZPL (785 nm). In order to properly model the molecule photo-physics, the metastable triplet state should be taken into account. Fluorescence is inhibited when the molecule is in its triplet state, which is hence responsible for blinking. However, this state is very unlikely populated in the case of DBT in Ac, with a probability (namely inter system crossing yield) ISC  $< 10^{-5}$ . c) Simplified sketch of the optical setup used for the measurement reported in the paper (details are presented in Section 6) and sketch of the device operated as single-photon source. Au, gold; AC, anthracene; DBT, dibenzoterrylene; PVA, polyvinyl alcohol.

single DBT molecules in Ac nanocrystals at low temperatures, the multilayer configuration discussed in ref. [20] is further adapted.

The SPS used in this work is obtained from an isolated DBT molecule, placed around 100 nm away from a metallic mirror (160 nm thick gold layer). This distance fits within the  $\lambda/(6n) \leftrightarrow \lambda/(4n)$  interval (where  $\lambda$  is the emission wavelength and  $n$  the refractive index of the medium), that is, the condition which maximizes the emission directionality within a small angle around the polar axis.<sup>[21]</sup> This simple configuration can be obtained with a cost-effective procedure, based on the deposition of DBT-doped Ac nanocrystals over the gold mirror. Such nanocrystals are prepared as suspension in water through a reprecipitation method<sup>[19]</sup> which enables a certain control over the crystal size and emitter concentration. For the device under investigation, we grow 200 nm thick nanocrystals containing single DBT molecules. The fabrication protocol is terminated by spin coating a 200 nm thick polyvinyl alcohol (PVA) layer, in order to stabilize the sample and flatten the interface between the dielectric layer and air.

Fine adjustment of the molecule distance with respect to the mirror is obtained by exploiting the almost flat statistics of their spatial distribution inside the host matrix. Indeed, the sample provides millions of SPSs, out of which few thousands appear brighter, due to their optimal placement and orientation with respect to the metallic mirror. Thanks to a very low probability of having more than one molecule per nanocrystal, such relevant cases correspond to the brightest spots of a fluorescent map such as the one shown in **Figure 1a**, obtained under wide-field illumination and imaging on camera.

In **Figure 1c**, a sketch of the optical setup is outlined, representing an epifluorescence microscope, where the sample is cooled

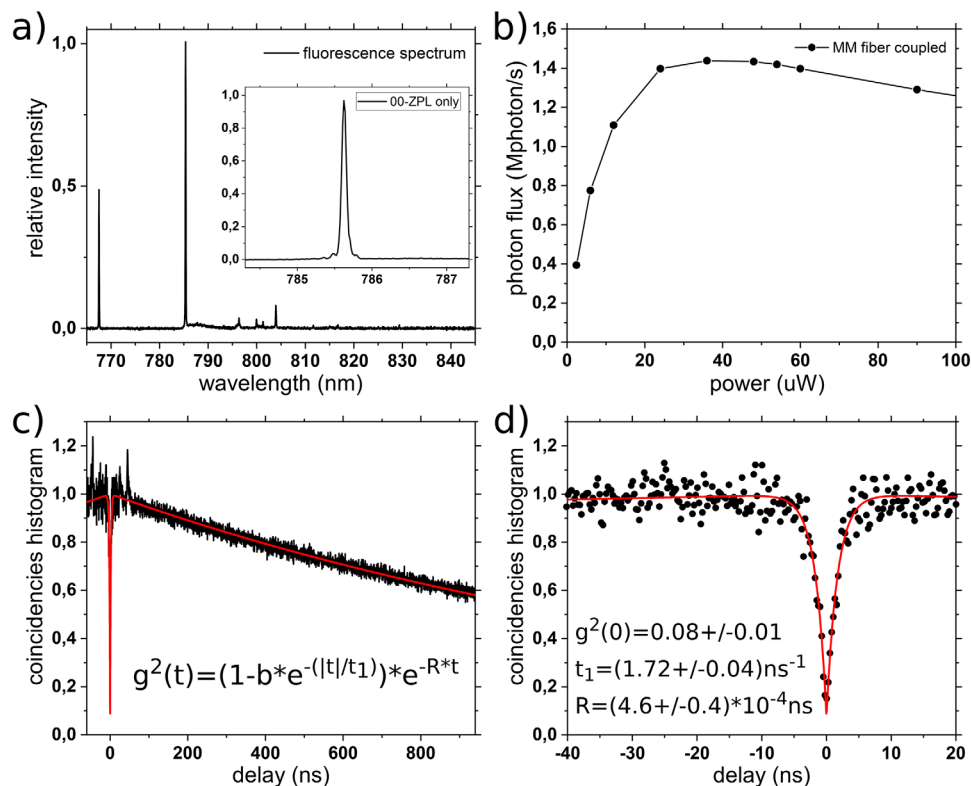


**Figure 2.** Metrological characterization of the molecule emission: a) Fluorescence spectrum, inset: fluorescence spectrum when filters are set to select a 2 nm wide spectral window around the molecule 00-ZPL (785.6 nm in this case). b) Photon flux detected with the SPAD as a function of the laser pump power. c) Normalized histogram of the inter-photon arrival times for maximum photon flux operation (30  $\mu$ W pump power). d) Zoom on the histogram in (c) around zero time delay, representing  $g^{(2)}(t)$ : the anti-bunching behavior shows the high purity of the single-photon stream. The red lines are a fit to the data with the expression shown in (c), while best estimation of the fit parameters is reported in (d).

down to 3 K and which is equipped with different detection options. More details about the optical setup are provided in Section 6.

Once a promising nanocrystal is selected, confocal illumination (and detection) is adopted for the optical characterization of the source. The use of isolated nanocrystals enables single emitter addressing without specific spatial filtering beyond confocal microscopy.

### 3. Metrological Characterization of the Molecule-Based Single-Photon Source

Single molecules are pumped into the first electronic excited state (which has a lifetime  $\tau \approx 4$  ns) via an auxiliary vibrational level using a diode laser centered at a wavelength of 767 nm (see Figure 1b). The Stoke-shifted fluorescence is filtered out and characterized in terms of the photon statistics and spectral features. In Figure 2a the emission spectrum of the molecule which is metrologically characterized and deployed in this paper is shown. The peak around 767 nm is due to the residual laser light, whereas the most intense signal is associated to the molecule main transition, that is, its 00-ZPL. This signal is then filtered in a bandwidth of about 2 nm around the wavelength  $\lambda \approx 785$  nm. In the inset of Figure 2a, the resulting spectrum appears limited by the spectrometer resolution ( $\approx 0.2$  nm) and

can be independently measured via excitation spectroscopy to be smaller than 100 MHz, that is, 1 pm.<sup>[19]</sup> The measurements reported in the following sections are obtained in these operative conditions.

A CW pumping scheme is employed in order to reach the highest average photon rates at the detector for a given overall efficiency. This implies a photon statistics becoming Poissonian for long integration times, unlike the case of pulsed operation (for which the variance in the number of emitted photons is ideally null for all times).

Both photon flux and  $g^{(2)}(t)$  function are measured at the output of a multi-mode fiber, as a function of the excitation power. Extract from the measurement results are depicted in Figure 2b–d, respectively.

The molecule-based SPS is able to deliver at the fiber-coupled detector up to  $1.4 \times 10^6$  photons/s, keeping high purity of the single-photon emission for any set rate (in particular,  $g^{(2)}(0) = 0.08 \pm 0.01$  at maximum photon rate, without deconvolving for the SPAD response function of around 0.4 ns). These characteristics are outstanding considering quantum emitters operated in the absence of optical cavities or local nano-structuring of the host material, especially in terms of the detected power in a given frequency interval. Indeed, according to the linewidth measurements reported in our previous works,<sup>[19]</sup> around 2/3 of the collected photon flux, that is, more than  $0.9 \times 10^6$  photons/s, falls within a 50 MHz wide spectral window.

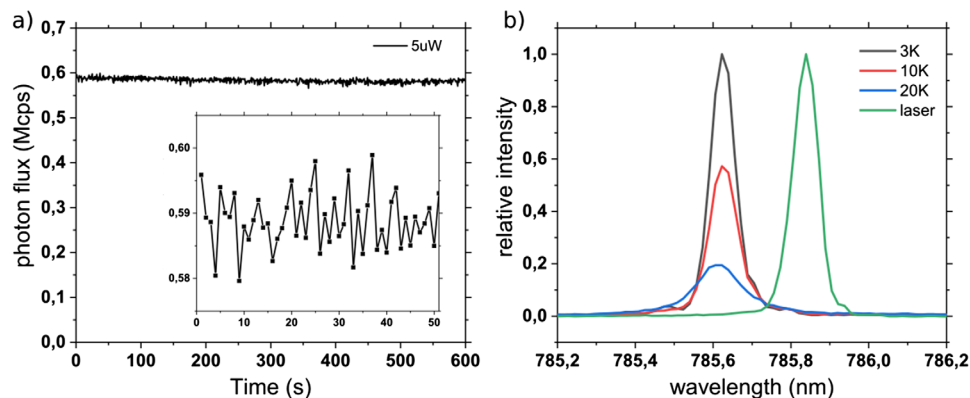


**Figure 3.** a) Temporal stability of the photon flux under CW excitation. A drift of around 2% due to the pump light alignment within a time interval of 10 min, and less than 1% fluctuations on a time-scale of few seconds (inset) is reported. b) Spectral response of the narrow-band line as a function of temperature, for a fixed pump power equal to 30  $\mu$ W. A lower absorption cross-section is observable already at 10 K, while spectral broadening is evident at higher temperature only, due to the limited spectrometer resolution ( $\approx 0.2$  nm estimation from laser line (green curve)).

It should be noted that the saturation curve reported in Figure 2b decays for very high pump powers. To the best of our knowledge, this behavior has not been reported before for organic molecules and is currently under investigation.<sup>[22]</sup> Among different possible explanations, there could be a power-dependent heating of the host matrix induced by the pump light, with a corresponding reduction of both the molecule absorption cross-section and emission branching ratio in the spectrally selected transition (ZPL). An alternative hypothesis relies on a more complex nonlinear dynamics occurring in the system, resulting in a power-dependent shelving effect. Despite the physical origin of such behavior, the accessible photon flux is sufficient for the proposed radiometric applications. An SPS brightness ( $B$ ) may also be defined as the relative probability of having a photon within the collection angle of the first lens with respect to the ideal case. A detailed discussion about brightness of the presented device and possible strategies for its optimization is provided for general interest in Section 6.

The photon statistics of the source presented in Figure 2c,d is obtained by measuring the histogram of the difference in the photon arrival times, using start and stop signals from two SPAD detectors, arranged in a Hanbury-Brown and Twiss (HBT) configuration (for details on the setup refer to Section 6 and Figure 5). It is well known that such data set represents correctly the  $g^{(2)}(t)$  only for short times. Indeed, for long times the coincidence probability is suppressed by the high detected count rate.

The  $g^{(2)}(t)$  function can be fitted with the expression

$$g^{(2)}(t) = (1 - b \cdot e^{-|t|/t_1}) \cdot e^{-Rt} \quad (1)$$

where  $b$  and  $t_1$  represent the depth and the time constant of the anti-bunching dip, respectively,<sup>[23]</sup> and the last term accounts for the arrival time probability, considering a Poissonian distribution ( $R$  is the average count rate per SPAD). We can exclude in first approximation a bunching contribution to the histogram profile given by the intermittency in fluorescence emission (blinking) occurring when the molecule falls in the metastable triplet state (see Figure 1b). Indeed, in DBT:Ac system this transition has a relative probability with respect to fluorescence emission smaller than  $10^{-5}$ , and the triplet lifetime is limited to few

**Table 1.** Attainable flux and purity of the single-photon stream for different temperatures.

Temperature [K]	Power <sup>a)</sup> [ $\mu$ W]	Max photon flux [Mphoton/s]	$g^{(2)}(0)$
3	30	1.36	0.08+/-0.01
5	42	1.27	
10	42	1.20	
15	42	1.09	0.06+/-0.02
15	72	1.19	
20	72	1.08	0.09+/-0.02

<sup>a)</sup> Power measured at the entrance of the objective lens.

microseconds.<sup>[17]</sup> These characteristics lead to dark periods of few microseconds separated by millisecond-long bright intervals, with a negligible bunching contribution to the  $g^{(2)}(t)$  profile. This assumption is confirmed by the agreement between the value for  $R$  obtained by the fit and the count rate directly read by each detector.

In the framework of metrological applications, it is relevant to determine also the stability of the photon flux over time. We report less than 1% fluctuations on short time-scales (seconds), and a drift of around 2% due to the pump light alignment within a time interval of 10 min (see Figure 3a).

Another set of measurements has been devoted to the determination of the highest temperature at which the device is able to guarantee a photon stream with reasonable optical properties for metrological applications (see discussion in Section 4).

Raising the temperature indeed, line-broadening is expected, together with a lowering of both the absorption cross-section and of the branching ratio into the 00-ZPL. In Figure 3b, the emission spectrum for different temperatures is shown for a fixed pump power. Due to the limited resolution of the spectrometer (evaluated to be around 0.2 nm by measuring a laser line with actual linewidth  $< 5$  MHz, that is,  $< 10$  fm), broadening of the line becomes evident only around 20 K. However, the combined effect of the other two aspects is effective already at 10 K and can be only partially mitigated by a stronger excitation. Table 1 gathers

the results of this analysis, which fixes the maximal operating temperature of the device to  $\approx 20$  K.

#### 4. Calibration of a Single-Photon Detector with a Molecule-Based SPS

Overall the developed source shows promising characteristics in order to operate as a secondary standard source for SPAD calibration.

Indeed, as a rule of thumb, an SPS delivering a photon stream with flux at detector  $> 1$  Mphoton/s,  $g^{(2)}(0) < 0.1$ , and spectrum FWHM  $< 2$  nm, yields comparable results in the calibration process as an attenuated laser. These figures arise from the following considerations: a photon flux of  $1 \times 10^6$  photons per second at a wavelength of  $\approx 785$  nm corresponds to  $\approx 250$  fW of optical power. As described in ref. [24], this power level is reasonably measurable with silicon photodiodes and is therefore set as a lower limit. The bandwidth limit of 2 nm reduces the measurement uncertainty associated with the spectral sensitivity of the silicon detector itself. Finally, a method based on the pulsed excitation of such a quantum emitter would get beyond the break-even point and become advantageous with respect to the use of attenuated laser pulses. In particular, under the condition  $g^{(2)}(0) = 0.1$ , the influence of multi-photon events on the measured detector efficiency would be comparable to the one obtained in the Poissonian regime for an average number of photon per detector dead time of 0.1.<sup>[8]</sup>

In this work, the detection efficiency of a Si-SPAD detector is determined by comparing the photon flux measurements of the SPS (see Section 2) performed with the SPAD detector (device under test) with an analog reference Si-detector. Details about the traceability chain for the calibration of the latter device are given in Section 6. The reference detector and the SPAD are equipped with a FC/PC fiber connector and their coupling efficiency is optimized for a multi-mode fiber. The photon flux measurements are performed sequentially. Thus, the SPAD detection efficiency  $\eta_{\text{SPAD}}$  is determined as  $\eta_{\text{SPAD}} = \frac{\langle N_{\text{SPAD}} \rangle}{\langle N_{\text{ref}} \rangle}$ , where  $N_{\text{SPAD}}$  is the count rate (counts/s) measured with the SPAD detector, while  $N_{\text{ref}}$  is the photon flux rate derived from the source optical flux measurement  $\Phi_s$  and the photon energy  $E$  ( $E = 2.53 \times 10^{-19}$  J for photon at 785.6 nm).  $\Phi_s$  is obtained as the ratio between the measured average photocurrent  $\langle I_f \rangle$  and the reference detector responsivity  $s_{\text{ref}}$ , and hence  $\langle N_{\text{ref}} \rangle = \frac{\langle \Phi_s \rangle}{E} = \frac{\langle I_f \rangle / s_{\text{ref}}}{E}$ .

Figure 4 shows the detection efficiency obtained for the SPAD detector (Perkin Elmer, SPCM-AQRH-13-FC) within the photon rate range from 0.144 to 1.32 Mphoton/s, which corresponds to an optical power range between 36.5 and 334 fW. To the best of our knowledge, such broad flux interval was never explored so far with an SPS, in the framework of detectors' calibration. Interestingly, the molecule emission rate approaches the regime in which the detector dead time ( $\tau_{\text{dead}}$ ) affects the measurement of the detection efficiency  $\eta_{\text{SPAD}}$ .<sup>[8]</sup>

The standard uncertainty associated with each measurement value is indicated by an error bar. It was calculated following the guidelines expressed in ref. [25]. The achieved uncertainty varies within the range from 2% to 6%, depending on the photon rate, that is, the lower the photon rate, the higher the un-

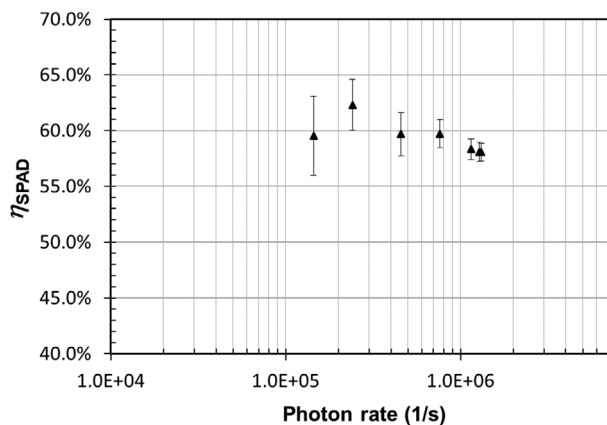


Figure 4. Calibration result for the SPAD detection efficiency (Perkin Elmer, SPCM-AQRH-13-FC) using the molecule-based single-photon source and a low-noise reference analog detector.

Table 2. Uncertainty budget for the Si-SPAD detection efficiency  $\eta_{\text{SPAD}}$  determined for an optical power of  $\approx 193$  fW, which corresponds to a photon flux rate of  $\approx 764$  kphoton/s. The model used for the estimation of the uncertainty is given by  $\eta_{\text{SPAD}} = \frac{hc}{\lambda} \cdot \frac{s_{\text{si}} F_{\text{Amp}} \text{SPAD}_{\text{Counts}}}{V_f (1 - F_{\text{Lin}})}$ , where  $h$  is the plank's constant,  $c$  is the speed of the light,  $\lambda$  is the wavelength,  $F_{\text{Amp}}$  is the amplification factor of the internal amplifier of the reference detector,  $V_f$  is the photo-voltage measurement (Si-detector measurement),  $F_{\text{Lin}}$  is the linearity factor correction of the Si reference detector and  $\text{SPAD}_{\text{Counts}}$  is the SPAD counts including dark counts correction.

Source of uncertainty	Standard uncertainty [%]
Planck's constant, $h$	—
Wavelength, $\lambda$	0.008
Speed of light, $c$	—
Si-detector spectral responsivity, $s_{\text{si}}$	0.400
Si-detector measurement, $V_f$	1.870
Amplification factor, $F_{\text{Amp}}$	0.100
Linearity factor of the Si-detector, $F_{\text{Lin}}$	0.030
Si-SPAD Counts, $\text{SPAD}_{\text{Counts}}$	0.020
<b>Combined uncertainty, <math>u_c</math></b>	<b>1.92</b>

certainty. This can be ascribed to the reference detector random noise, which is the highest contribution to the total uncertainty at fW levels, as observed in the uncertainty budget shown in Table 2. The final value obtained for the Si-SPAD quantum efficiency is  $\eta_{\text{SPAD}} = (0.603 \pm 0.012)$ .

#### 5. Conclusions

In this paper we demonstrate the realization of an absolute SPS based on the emission of an organic dye molecule operated at cryogenic temperature. This result is obtained by linking the single-photon stream generated by the molecule to a national radiometric standard for optical fluxes via an analog Si-detector, calibrated through an unbroken traceability chain and able to read optical radiant fluxes down to a few tens of fW. The source presented here shows significant advances with respect to

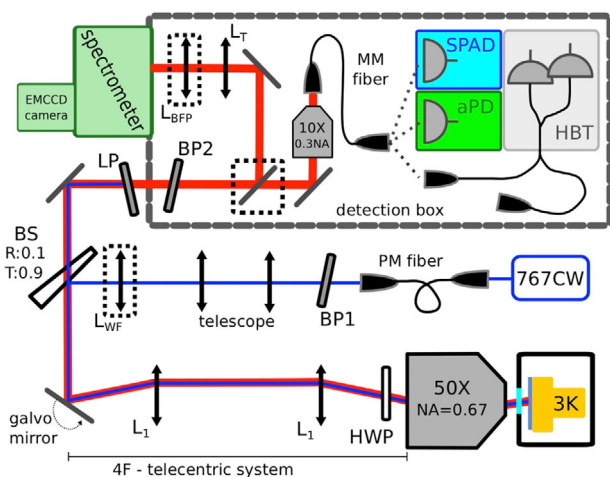


**Figure 5.** Detailed sketch of the optical setup: dashed squares mark flippable elements. PM, polarization maintaining fiber; BP, bandpass filter;  $L_{WF}$ , lens for wide-field imaging; BS, beam sampler;  $L_1$ , lenses for telecentric system; HWP, half wave plate; LP, longpass filter;  $L_T$ , tube lens;  $L_{BFP}$ , lens for back focal plane imaging; MM, multi-mode fiber; SPAD, single photon counting module; aPD, analog Si photodiode; HBT, fiber-based Hanbury-Brown and Twiss interferometer.

previous demonstrations in the field of radiometry in terms of flux (1.32 Mphoton/s), linewidth ( $<0.2$  nm) and purity ( $g^{(2)}(0) < 0.1$ ) of the emission.

The traceably measured optical radiant flux adjustable between 37 and 334 fW at a wavelength of  $(785.6 \pm 0.1)$  nm is unprecedented and allows the direct calibration of a single-photon detector (SPAD) through comparison with calibrated high-sensitivity analog Si detector for the first time.

The reported SPS can in principle be operated in pulsed conditions, with an estimated photon flux of around 5 Mphoton/s at first lens ( $NA = 0.67$ ) for 50 MHz pump repetition rate. Under these conditions the device can work as a predictable true SPS, whose photon flux is directly tuned by acting on the pump repetition rate, with high reliability and precision also at power levels below the detection limit of conventional photodetectors. The developed device may hence realize a standard source for quantum radiometry, complementing the blackbody radiator and the synchrotron radiation source in the low-photon-flux regime.

Thanks to the long coherence time and the efficient molecular emission into the Fourier-limited 00-ZPL, the presented device might find immediate applications also for quantum communication, simulation and computing, or in quantum imaging.

## 6. Experimental Section

**Optical Setup:** The epifluorescence microscope setup used in the experiment is shown schematically in **Figure 5**. For CW excitation of the DBT molecules, an external cavity diode laser operating at a wavelength of 767 nm (Toptica DLX110) was employed. The laser beam was first spatially filtered (through coupling into a PM fiber, Thorlabs P3-780PM-FC) in order to fit a Gaussian profile; then it was spectrally filtered (with the bandpass filter BP1, Semrock Brightline FF01-769/41) in order to avoid residual emission at the detection wavelength leaking into the detection path; finally it was mode matched with the objective lens back entrance (SigmaKoki PAL-50-NIR-HR-LC07,  $NA = 0.67$ , transmission at 785 nm = 0.7)

**Table 3.** Photon loss budget table.

Element	Efficiency	Symbol
Cryostat windows	0.85	
Objective transmission	0.7	
Beam splitter	0.9	
Spectral filters <sup>a)</sup>	0.85	
Mirrors and lenses <sup>b)</sup>	0.54	
Fiber coupling <sup>c)</sup>	0.75	
<b>Overall optical setup</b>	<b>0.18</b>	$\beta_{opt}$
<b>Photon flux detector</b>	<b>0.6</b>	$\beta_{det}$
HBT detectors	0.65	
<b>Collection (<math>NA = 0.67</math>)<sup>d)</sup></b>	<b>0.35</b>	$\beta_{col}$

<sup>a)</sup> Residual losses due to close proximity of filters' edges; <sup>b)</sup>  $9\times$  metallic mirrors;  $5\times$  spherical lenses; <sup>c)</sup> Objective lens transmission @785 nm = 0.8; coupling to fiber  $\approx 0.94$ ; <sup>d)</sup> Collection obtained with  $NA = 0.67$  objective lens according to simulations.<sup>[20]</sup>

through the appropriate two-lens telescope, in order to exploit the available numerical aperture and minimize the size of the confocal spot (evaluated around  $1 \mu\text{m}$  in diameter). A beam sampler BS (Thorlabs BSF20-B) with  $\approx 0.1/0.9$  reflection/transmission coefficients was used to reflect the light toward the objective lens and conversely transmit the incoming signal. In the common path, a telecentric lens system linking a mirror with motorized tilt and the objective back entrance allowed for exploration of the sample without the need for a translational stage. Another converging lens can be added before the BS if wide-field illumination was required ( $L_{WF}$ ). The sample was fixed in thermal contact with the cold finger of a closed-loop liquid-helium cryostat (Montana Instrument) and kept at 3 K, and was optically addressable through a double window for a total glass thickness of 0.7 mm. The objective lens in use was designed to compensate for that.

The signal transmitted by the BS was directed toward the detection box, which was equipped at its entrance with a longpass filter (LP, Semrock RazorEdge LP02-785RE-25) to filter out the laser light back reflected by the sample. A second bandpass filter (BP2, Semrock TBP01-790/12), whose transmission window can be shifted to the blue by tilting, was added in the detection path if selection of the 00-ZPL line was required. The photon flux was hence redirected to a fiber coupling system consisting in a low magnification objective lens (Olympus UPlanFL N,  $10\times$ ,  $NA = 0.30$ , transmission at 785 nm = 0.8) focusing light into a cleaved multi-mode fiber (Thorlabs M42L02, core diameter:  $50 \mu\text{m}$ ,  $NA = 0.22$ ). The fiber can deliver the photon stream to either a low-noise analog Si detector (Femto FWPR-20-s), or to a calibrated Si SPAD (Perkin Elmer SPCM-AQR-13-FC), or to a couple of SPAD in HBT configuration (Excelitas 800-14-FC) through a fibered beam splitter (Thorlabs FCMM625-50A-FC). The latter arrangement, with the help of a time-correlated single-photon counting system (PicoQuant PicoHarp 300), gave access to the second-order autocorrelation function of the photon stream  $g^{(2)}(t)$  in the form of time delay histogram of the detection events between the two detectors.

Finally, a flippable mirror set before the fiber coupling system can deviate the signal beam toward an EM-CCD-equipped spectrometer (Andor Shamrock SR-303i-A, camera iXon3), which can work also as simple wide-field imaging camera (tube lens  $L_T$  focal length 20 cm). By adding a second converging lens  $L_{BFP}$  at the appropriate position between the tube lens and the camera, imaging of the back focal plane of the objective lens was obtained.

The photon loss budget is shown in **Table 3**, which reports the efficiency of each element in the setup.

**Emitter Brightness and Coherence Properties:** The brightness of the SPS can be evaluated by comparing the count rate CR read by the SPAD with the ideal maximal rate of the source SR (corresponding to the inverse of the excited state lifetime in case of CW excitation). The two rates are

related through the expression  $CR / SR = \beta_{det} \beta_{opt} \beta_{col} \beta_{mol} P$ , where  $\beta_{det}$  is the quantum efficiency of the detector,  $\beta_{opt}$  is the overall optical setup efficiency,  $\beta_{col}$  the collection efficiency of the first lens (objective) considering all radiative and non-radiative losses,  $\beta_{mol}$  the probability for the molecule to emit a stored excitation as a photon in the ZPL, and  $P$  accounts for the efficacy of the pumping illumination. Consequently, the brightness at first lens was determined as  $B = \beta_{col} \beta_{mol} P = CR / SR / \beta_{det} / \beta_{opt}$ .

According to the photon flux characterization presented in Section 3, the detector efficiency determined in Section 4, and the overall optical setup efficiency ( $\beta_{opt} \approx 0.18$ ), the brightness of the source at first lens (for  $NA = 0.67$ ) amounts approximately to  $B \approx 3.5\%$ .

Concerning the coherence of the emission, a ZPL linewidth of  $(65 \pm 20)$  MHz, measured by excitation spectroscopy on a statistical ensemble of molecules in samples like the one under investigation was reported. This value is quite close to the natural Fourier-limited value of  $(36 \pm 3)$  MHz, corresponding to the average lifetime of the excited state  $\tau = (4.4 \pm 0.4)$  ns, obtained from  $g^{(2)}(\tau)$  measurements at low pumping rate. The residual dephasing contribution was attributed to the operating temperature (3 K), which is close to the activation temperature for DBT:Ac system.<sup>[16]</sup>

In order to evaluate the potentiality of the device, the attainable brightness and photon flux in case of optimal operation is considered.

- 1) From semi-analytic simulations,<sup>[20]</sup> the collection efficiency was estimated with our objective to be around  $\beta_{col} \approx 0.35$ , which leads to a source quantum efficiency  $\beta_{mol} P \approx 10\%$ . This value is much lower than the 40% expected from the literature, and this mismatch was attributed to the anomalous behavior presented in Section 3. In other words, it was believed that with the current pumping scheme we were not able to achieve maximum efficiency either because of a non-unitary population of the electronic excited state, and/or because the branching ratio into the narrow ZPL was reduced by a power-induced heating of the system. Depending on the origin of the photon flux dimming at high power, different strategies can be applied to mitigate the effect. In case the consequences of a local heating of the host matrix were faced, a bath cryostat would help in terms of cooling power. Alternatively, off-resonance pulsed operation is expected to avoid completely the issue provided that the average impinging power was smaller than  $20 \mu W$ . In case of multi-photon dynamics, resonant excitation combined with cross-polarized detection should allow efficient pumping for power well below the level of activation of the detrimental effect;
- 2)  $\beta_{col}$  can be increased exploiting higher NA objective lenses (e.g.,  $\beta_{col} \approx 0.45$  for  $NA = 0.8$  was estimated);
- 3) In a dedicated optical setup with optimized AR coatings, filters, and optical path length, the overall optical setup efficiency can easily be pushed to  $\beta_{opt} = 0.6$ ;
- 4) Finally, it was demonstrated in ref. [20] that with the addition of a second metallic layer on top of the Ac nanocrystals, for the appropriate thickness and distance from the bottom mirror, the emission of the molecule can be further redirected toward the polar axis, resulting in  $\beta_{col} \approx 0.55$  for the considered NA

According to the considerations reported above,  $B \approx 13\%$  and a photon flux at first lens (detector) of  $\approx 7$  Mphoton/s (4 Mphoton/s) for 50 MHz pump repetition rate is expected with the present device. A factor 1.5 enhancement for both quantities is envisioned for the next generation of devices, based on the argument introduced above (point 4).

**Traceability Chain for the Calibration of the Reference Si-Detector.** The reference detector used for the photon flux measurement of the source was an analog ultra-low-noise Si-detector (Femto FWPR-20-s). It consisted of a fiber-coupled Si photodiode of  $1.1 \times 1.1 \text{ mm}^2$  active area and a trans-impedance amplifier with gain of  $1 \times 10^{12} \text{ V A}^{-1}$ . The minimum noise equivalent power (NEP) of the detector was  $0.7 \text{ fW Hz}^{-1/2}$ . Its spectral responsivity  $s_{Si}(\lambda)$  was determined by calibrating it against a working standard traceable to PTB's primary standard for optical power, that is, the cryogenic radiometer.<sup>[26]</sup> The complete traceability chain is shown in **Figure 6**, where  $\lambda_i$  is the wavelength,  $\Phi$  is the optical radiant flux, and  $u$  is the standard measurement uncertainty. In a first step, a Si trap detector was calibrated against the cryogenic radiometer at specific wave-

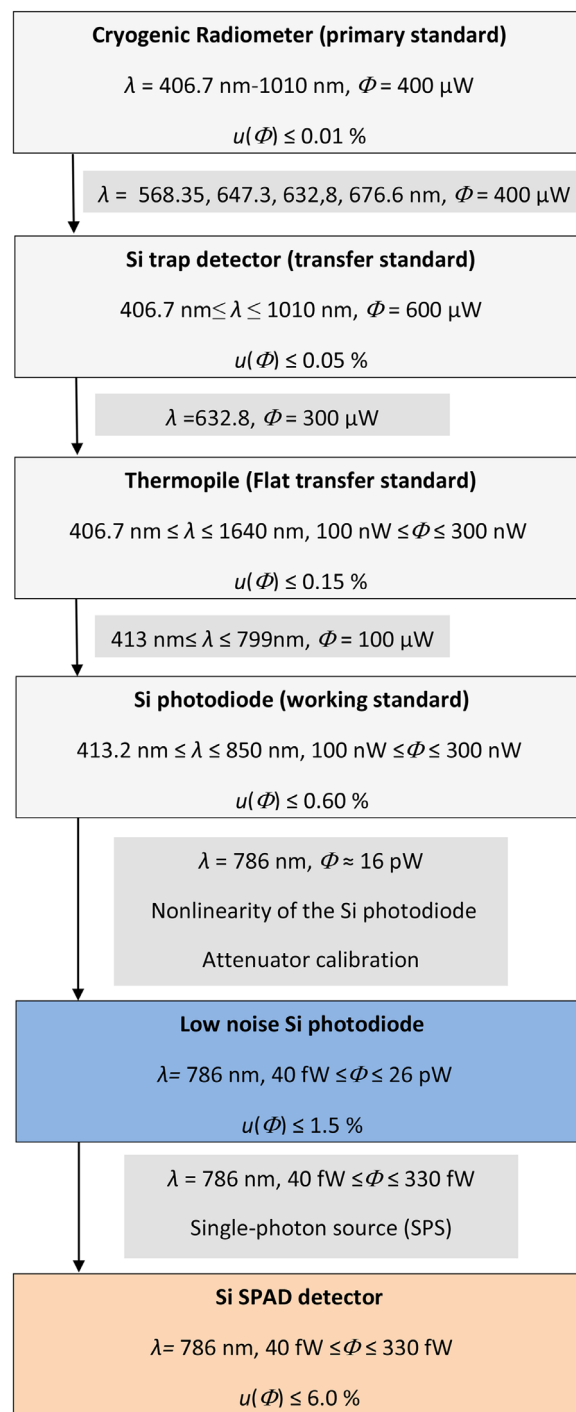


**Figure 6.** Traceability chain for the calibration of the low-noise analog Si-detector, and the additional link reported in this paper, which opens to the traceability of optical power flux down to few hundreds of aW.

lengths and optical powers ( $\mu W$ ). Then, a spectrally flat detector, that is, a thermopile detector, was used to determine the responsivity of a Si photodiode, which acts as working standard at the specific wavelength of the photons emitted by the SPS, that is, 785.6 nm. Finally, the spectral responsivity of the low-noise Si-detector used for the calibration of the Si-SPAD detector was obtained by means of the double attenuation



calibration technique described in ref. [8] and the Si photodiode working standard. The spectral responsivity obtained at 785.6 nm is

$$s_{\text{Si}} = (57.52 \pm 0.58) \times 10^{(-2)} \text{AW}^{-1} \quad (2)$$

The uncertainty of the spectral responsivity here reported corresponds to a standard uncertainty ( $k = 1$ ).

## Acknowledgements

The work reported on this paper was funded by the project EMPIR 17FUN06 SIQUST. This project received funding from the EMPIR program co-financed by the Participating States and from the European Union Horizon 2020 research and innovation program. The copyright line for this article was changed on February 26, 2020 after original online publication.

## Conflict of Interest

The authors declare no conflict of interest.

## Keywords

quantum radiometry, single molecules, single-photon detectors, single-photon sources

Received: July 12, 2019

Revised: September 4, 2019

Published online: October 22, 2019

- [1] J. L. O'Brien, A. Furusawa, J. Vuckovic, *Nat. Photonics* **2009**, *3*, 687.
- [2] J.-Y. Hu, M.-Y. Jing, L.-T. Xiao, S.-T. Jia, G.-Q. Qin, G.-L. Long, *Light: Sci. Appl.* **2016**, *5*, e16144.
- [3] D. Gatto Monticone, K. Katamadze, P. Traina, E. Moreva, J. Forneris, I. Ruo-Berchera, P. Olivero, I. P. Degiovanni, G. Brida, M. Genovese, *Phys. Rev. Lett.* **2014**, *113*, 143602.
- [4] a) A. Peruzzo, M. Lobino, J. C. F. Matthews, N. Matsuda, A. Politi, K. Poullos, X.-Q. Zhou, Y. Lahini, N. Ismail, K. Wörhoff, Y. Bromberg, Y. Silberberg, M. G. Thompson, J. L. O'Brien, *Science* **2010**, *329*, 1500; b) H. Wang, Y. He, Y.-H. Li, Z.-E. Su, B. Li, H.-L. Huang, X. Ding, M.-C. Chen, C. Liu, J. Qin, Jin-Peng Li, Y.-M. He, C. Schneider, M. Kamp, C.-Z. Peng, S. Höfling, C.-Y. Lu, J.-W. Pan, *Nat. Photonics* **2017**, *11*, 361.
- [5] N. Sangouard, H. Zbinden, *J. Mod. Opt.* **2012**, *59*, 1458.
- [6] a) C. J. Chunnillall, I. P. Degiovanni, S. Kück, I. Müller, A. G. Sinclair, *Opt. Eng.* **2014**, *53*, 081910; b) J. Zwinkels, A. Sperling, T. Goodman, J. Campos Acosta, Y. Ohno, M. L. Rastello, M. Stock, E. Woolliams, *Metrologia* **2016**, *53*, G1.
- [7] W. Schmunk, M. Rodenberger, S. Peters, H. Hofer, S. Kück, *J. Mod. Opt.* **2011**, *58*, 1252.
- [8] M. López, H. Hofer, S. Kück, *J. Mod. Opt.* **2015**, *62*, 1732.
- [9] J. Y. Cheung, C. J. Chunnillall, E. R. Woolliams, N. P. Fox, J. R. Mountford, J. Wang, P. J. Thomas, *J. Mod. Opt.* **2007**, *54*, 373.
- [10] B. Lounis, M. Orrit, *Rep. Prog. Phys.* **2005**, *68*, 1129.
- [11] G. Loudon, *Quantum Theory of Light*, Oxford University Press, Oxford, UK **2000**.
- [12] B. Rodiek, M. Lopez, H. Hofer, G. Porrovecchio, M. Smid, X.-L. Chu, S. Götzinger, V. Sandoghdar, S. Lindner, C. Becher, S. Kueck, *Optica* **2017**, *4*, 71.
- [13] A. Vaidu, G. Porrovecchio, X.-L. Chu, S. Lindner, M. Smid, A. Manninen, C. Becher, V. Sandoghdar, S. Götzinger, E. Ikonen, *Metrologia* **2017**, *54*, 218; and erratum in *Metrologia* **2017**, *54*, 417.
- [14] P. Senellart, G. Solomon, A. White, *Nat. Nanotechnol.* **2017**, *12*, 1026.
- [15] G. Wrigge, I. Gerhardt, J. Hwang, G. Zumofen, V. Sandoghdar, *Nat. Phys.* **2008**, *4*, 60.
- [16] a) A. A. L. Nicolet, B. Kozankiewicz, C. Hofmann, M. Orrit, *ChemPhysChem* **2007**, *8*, 1929; b) C. Toninelli, K. Early, J. Bremi, A. Renn, S. Goetzinger, V. Sandoghdar, *Opt. Express* **2010**, *18*, 6577; c) B. Kozankiewicz, M. Orrit, *Chem. Soc. Rev.* **2014**, *43*, 1029.
- [17] A. A. L. Nicolet, C. Hofmann, M. A. Kol'chenko, B. Kozankiewicz, M. Orrit, *ChemPhysChem* **2007**, *8*, 1215.
- [18] a) J.-B. Trebbia, P. Tamarat, B. Lounis, *Phys. Rev. A* **2010**, *82*, 063803; b) S. Grandi, K. D. Major, C. Polissen, S. Boissier, A. S. Clark, E. A. Hinds, *Phys. Rev. A* **2016**, *94*, 063839.
- [19] S. Pazzagli, P. Lombardi, D. Martella, M. Colautti, B. Tiribilli, F. S. Cataliotti, C. Toninelli, *ACS Nano* **2018**, *12*, 4295.
- [20] S. Checcucci, P. Lombardi, S. Rizvi, F. Sgrignuoli, N. Grhuler, F. B. C. Dieleman, F. S. Cataliotti, W. H. P. Pernice, M. Agio, C. Toninelli, *Light: Sci. Appl.* **2017**, *6*, e16245.
- [21] C. A. Balanis, *Antenna Theory: Analysis and Design*, 3rd ed., John Wiley & Sons, Hoboken **2005**.
- [22] P. Lombardi, F. Piccioli, M. Colautti, H. Schauffert, C. Toninelli, in preparation.
- [23] Parameters  $b$  and  $t$  are related to  $g(0)$  and  $\tau$  as follows:  $g^{(2)}(0) = 1 - b$ ;  $1/t_1 = 1/\tau + P$ , where  $P$  is the pump rate.
- [24] G. Porrovecchio, M. Šmid, M. López, H. Hofer, B. Rodiek, S. Kück, *Metrologia* **2016**, *53*, 1115.
- [25] *Guide to the Expression of Uncertainty in Measurement*, 1st ed., BIPM, September **2008**.
- [26] L. Werner, J. Fischer, U. Johannsen, J. Hartmann, *Metrologia* **2000**, *37*, 279.